Progress in Organic Coatings 150 (2021) 105969

Contents lists available at ScienceDirect

Progress in Organic Coatings

journal homepage: www.elsevier.com/locate/porgcoat

Enabling zero added-coalescent waterborne acrylic coatings with cellulose nanocrystals

Ezgi M. Dogan-Guner [a,*], Stan Brownell [b], Gregory T. Schueneman [c], Meisha L. Shofner [d], J. Carson Meredith [a,*]

[a] School of Chemical and Biomolecular Engineering, Georgia Institute of Technology, Atlanta, GA, USA
[b] Dow Coating Materials, The Dow Chemical Company, Collegeville, PA, USA
[c] Forest Products Laboratory, U.S. Forest Service, Madison, WI, USA
[d] School of Materials Science and Engineering, Georgia Institute of Technology, Atlanta, GA, USA

ARTICLE INFO

Keywords:
Polymer nanocomposite
Cellulose nanocrystal
Waterborne acrylic coatings
Volatile organic compound
Coalescent

ABSTRACT

Waterborne acrylic coatings contain volatile and non-volatile coalescents. Volatile organic compound (VOC) coalescents enable film formation of hard acrylic polymers at ambient temperature, but their evaporation results in air pollution and health concerns. Non-volatile alternatives are available, but they remain in the coating long-term and as a result films are often tacky and lack adequate hardness. Reinforcing mineral fillers are available, but are associated with sustainability challenges inherent to mineral mining. An alternative approach demonstrated here utilizes a renewably-sourced, plant-based hardening filler dispersed in the water phase, with soft polymer latexes that don't require VOCs for film formation. We reinforced coalescent-free and ambient film-forming butyl acrylate/methyl methacrylate/methacrylic acid latexes with cellulose nanocrystals (CNCs) by a post-synthesis blending approach. CNCs possess high elastic modulus and tensile strength, making them promising candidates to improve the mechanical performance of soft ambient film-forming acrylic latexes. CNCs form aggregates within the interstices between latex particles as water dries, however film coalescence is not compromised. Films with 15 wt% CNC showed almost 230 % improvement in Koenig hardness and 10x improvement in the nanoindentation hardness compared to neat films, achieving properties similar to hard VOC-containing acrylic binders in a zero-added VOC formulation.

1. Introduction

Paints and coatings with a market of ~43 million tons in 2016 [1], have annual volatile organic compound (VOC) emissions of ~2 million tons [2]. Reducing VOC release has driven development of waterborne paints, but despite advances many interior waterborne products contain 250 g/L VOCs [3]. In addition to inherent health effects [4], VOCs react with atmospheric nitrogen oxides, forming ground-level ozone [5] that contributes to global warming and harms health [6]. Coating producers are under increasing pressure to decrease VOC content because of legislation and customer demand. However, transitioning to low VOC products brings a challenge known as the "film formation dilemma", in which the VOC organic coalescents are needed to plasticize individual latex particles so that they form hard, durable coatings following VOC evaporation.

Acrylics are the most used binder resin in waterborne coatings. Hardness of the acrylic is an important aspect of coating durability. Soft latex particles that easily coalesce to form a film lack adequate hardness. Latexes are often formulated with copolymers with high glass transition temperature (T_g) but VOC coalescents are added to temporarily plasticize the particles to enable film formation at ambient conditions [7]. Industry also employs non-evaporative plasticizers that provide coalescence. However, the film remains tacky after curing. Thus, alternative approaches are desired to achieve the performance of high T_g acrylic latex coatings in the lower VOC formulations of today.

One approach is to add a hardening filler to the polymer matrix. Mechanically robust nanoscale fillers have been shown to improve polymer mechanical performance [8], including nanoscale fillers such as clay [9], silica [10], and carbon nanotubes [11]. Cellulose nanocrystals (CNCs) are proposed as a renewable filler to enhance mechanical performance of soft latex films, due to their high crystallinity, strength, and modulus, low density (relative to mineral fillers), and optical transparency (when

* Corresponding authors.
E-mail addresses: ezgidg@gatech.edu (E.M. Dogan-Guner), carson.meredith@chbe.gatech.edu (J.C. Meredith).

https://doi.org/10.1016/j.porgcoat.2020.105969
Received 16 June 2020; Received in revised form 1 September 2020; Accepted 9 September 2020
Available online 5 October 2020

dispersed adequately or matched to the matrix refractive index) [12–14]. In contrast to mineral or synthetic based fillers mentioned above, CNCs are plant-based, highly ordered rod-shaped particles with high elastic moduli in the range of 100−150 GPa [15]. Due to anionic sulfate half-ester surface groups, these CNCs form a charge-stabilized dispersion in water. As a result, they can be readily added to waterborne polymers as a reinforcing filler [16,17]. Indeed researchers [18–20] have observed improved coating hardness by blending CNC dispersions with acrylic latexes, but unfortunately these studies used VOCs or otherwise did not quantify VOC content. Abitbol et al. [18] and Pu et al. [19] used a commercial latex containing approximately 10 wt% coalescent and 100 g/L VOC, respectively.

We report a simple method of adding unmodified CNCs to enhance the mechanical performance of ambient film-forming acrylic coatings that have zero added coalescent. Compared to *in situ* polymerization with CNCs, this approach does not require surface functionalization or copolymerization with CNCs. VOC content of the latex used in this work was measured to be ~0.64 g/L (Table S1), whereas the threshold VOC limits are 50 g/L for low-VOC and 5 g/L for zero-VOC labeled paints. In addition to the use of an ambient film-forming binder with zero added coalescent, a difference relative to previous work is the use of latexes containing methacrylic acid (MAA) to introduce carboxylic functional groups that promote interactions with CNCs. Wood-derived CNCs were blended into these latexes at different loadings. We characterized the resulting acrylic latex/CNC films to determine the film formation, the morphology of CNCs in the latex matrix, and mechanical performance in order to demonstrate that CNCs enable zero VOC binder formulations with mechanical performance similar to VOC-containing hard acrylics.

2. Experimental

2.1. Materials

2.1.1. Aqueous CNC dispersion

An aqueous CNC dispersion (5.5 wt%, Na^+ form, USDA Forest Service Forest Products Laboratory, Madison, WI) was used as received. The dispersion was prepared from mixed southern yellow pine dissolving pulp via 64 % sulfuric acid digestion, described elsewhere. [21] The CNCs had 0.86 wt % sulfur (dry basis) due to sulfate half-ester groups from the hydrolysis.

2.1.2. Waterborne acrylic latex formulations

Two well-characterized coalescent-free latexes with a solid content of 39.4 wt% were prepared by emulsion polymerization of butyl acrylate (BA), methyl methacrylate (MMA), and MAA. The monomers were emulsified with sodium lauryl sulfate (SLS) and polymerized with thermally-initiated ammonium persulfate at 87 °C for 120 min. The pH was adjusted to 7.0–8.0 with dilute ammonium hydroxide to provide long term colloidal stability. Additional details are provided in Supporting Information (Table S2). The two latexes are denoted as MAA5 and MAA10, corresponding to MAA content. MAA5 contained 60 % BA, 35 % MMA, and 5% MAA. MAA10 contained 65 % BA, 25 % MMA, and 10 % MAA. MAA assists electrostatic stabilization of polymer particles. The higher MAA fraction makes the polymer particles more hydrophilic due to −COOH functional groups, with a goal of promoting compatibility with CNCs. Carboxylic acid co-monomers were previously found to increase shear strength of acrylic latex films due to intermolecular dipole-dipole interactions of acid groups. [22,23] Hydrogen bonding between carboxylic acid groups with hydroxyl groups on CNCs was also demonstrated [24,25].

2.2. Preparation of composite films

Acrylic latex/CNC composites were prepared by post-synthesis blending. Figure S1 shows a schematic representation of physical blending and a composite film. The aqueous CNC dispersion (5.5 wt%) was blended into the MAA5 and MAA10 latexes. Different amounts of CNC dispersion (0–18.9 g) were added to 15 g of base latex to change the CNC loading (0−15 wt%) in the dry films. Additional information is provided in Table S3. The resulting mixture was vortexed for 1 min (IKA Vortex3). Vortex method resulted in better dispersion compared to use of magnetic stirrer (Figure S2). A mixing time of 1 min was sufficient to obtain a homogeneous dispersion of CNCs in the latexes. The latex samples were cast on 0.25 cm thick glass substrates (10cm × 10cm) with a Gardco drawdown plate and an Elcometer 3540 film applicator to obtain 300 μm thick wet coatings. Coatings were dried overnight resulting in dry films with thicknesses ranging from 90 to 180 μm depending on the solid content (Table S3).

2.3. Characterization of CNC dispersion and latexes

A Bruker Icon AFM was used to image individual CNCs. The CNC/water dispersion was diluted with DI water to 0.001 wt% and blade coated onto a cleaned silicon wafer. Images were analyzed by using Gwyddion software to obtain length and height for individual CNCs. 50 isolated particles were measured from 10 different AFM topography images. The cross section of CNCs was taken as the height at the center of its length to avoid tip-broadening effects.

A Malvern Zetasizer Nano ZS90 was used to measure the zeta potential and average particle size of the CNC dispersion and latexes. For particle size distribution, the CNC/water dispersion was used as received and latexes were diluted with DI water to 0.025 wt%. From three measurements the z-average intensity-weighed mean diameter of particles was determined. Average zeta-potential was determined from three measurements on 10 μl CNC dispersion and latexes diluted with 2 ml DI water.

A Mettler Toledo Seven2Go pH/mV meter was used to measure the pH of CNC dispersion and latexes.

2.4. Characterization of CNC and latex films

A silicon cantilever with rotated tip (8 nm radius) was used in an AFM (Veeco, Dimension 3100) to study dry film surface topography. The AFM probe had a nominal spring constant and frequency of 1.6−6 N/m and 50−100 kHz, respectively. Height and amplitude images were captured with tapping mode in air. Roughness values (rms) were determined on 500 nm x 500 nm square areas.

T_g values of neat and 15 wt% CNC films were measured by DSC (TA Instruments DSC Q200). Samples were equilibrated at −50 °C and heated to 150 °C under nitrogen at 10 °C/min. The midpoint T_g was measured to capture the as-processed structure.

Minimum film formation temperatures (MFFTs) of all composite films were measured visually based on the change in optical clarity upon film formation, over a temperature range from -5 to 13 °C in desiccated air.

The water content of latex films was evaluated with thermogravimetric analysis (TGA - TA Instruments Q5000). Neat, 5 wt% and 15 wt% CNC samples were heated from room temperature to 400 °C at 10 °C/min.

CNC composition in the films was evaluated with ATR-FTIR (Nicolet iS50 with diamond ATR crystal). The scan range was 4000 cm^{-1} – 600 cm^{-1} with a resolution of 4 cm^{-1} and a total of 64 scans. Two randomly-chosen locations were scanned on the films for each composition and we found no difference (paired *t*-test with $\alpha = 0.05$) between spectra at these locations. The spectra were normalized at the 1725 cm^{-1} peak associated with carbonyl groups in acrylic polymers.

Polarized light microscopy (PLM) was used to assess the dispersion of CNC in acrylic films by observing birefringence in transmission under crossed polarizer and analyzer (Olympus BX51).

The cross-sections of the films were characterized using FE-SEM (Zeiss Ultra60). Latex films were cryo-fractured by immersing in liquid nitrogen, and surfaces were sputter-coated with gold and imaged at 3 kV.

Optical transparency of the films was assessed by light transmission over wavelengths of 200−800 nm with a UV–vis spectrometer (Shimadzu UV-1800). Transmittance values were normalized to a film thickness of 100 μm by using the Beer-Lambert law.

A high-throughput mechanical characterization (HTMECH) instrument [26], was used to deform films biaxially with a 1.25 mm diameter hemispherical indenter normal to the film plane at a speed of 10 mm/s. The average ultimate tensile strength (UTS) and strain at break were reported from five stress-strain curves per sample.

Uniaxial tensile testing was performed (Instron 5566) to obtain modulus, by using crosshead displacement data, for relative comparison among samples. Three films prepared by using a 'dog bone' cutting die for the ASTM D-1708 geometry were tested for each composite composition at lab conditions (approximately 20 °C and 26 % relative humidity) with a strain rate of 10 mm/min.

A Hysitron TriboIndenter equipped with a Berkovich diamond indenter was used in a load-controlled mode to indent neat and CNC loaded latex films at room temperature at loads between 200−500 μN with 100 μN increments. A polycarbonate reference was used to determine the area function of the indenter tip. A triangle load function was used with constant indentation time. Four indentations were performed on each film.

Pencil hardness was measured with an Elcometer 501 test kit by ASTM D3363. The reported hardness is the hardest pencil grade that doesn't cut the coating at 45°, based on testing each film twice.

Koenig hardness was measured on the first and seventh day of drying for coatings cast on aluminum Q panels by using a TQC pendulum tester (Model SP0500). The average measurement from three spots on the panels is reported.

3. Results and discussion

3.1. Characterization of CNC dispersion and composite latexes

Figure S3 shows latex/CNC mixtures (MAA5 post-blends for 0−5 wt % CNC loadings). The pH, average particle size, and zeta potential of the CNC dispersion, neat latexes, and latex/CNC blends are provided in Table S4. The pH of the latexes remained the same after the addition of the CNC dispersion. Latex dispersions remained stable after addition of CNCs in all cases (Table S4). The particle sizes of neat MAA5 and MAA10 latexes measured by DLS were similar, 117 ± 2 nm and 116 ± 1 nm, respectively. The addition of CNCs had a negligible impact on latex particle sizes, suggesting that CNCs do not aggregate on latex particles in suspension, consistent with their electrostatic charge. The zeta potential of the aqueous CNC dispersion (5.5 wt%) was measured to be −47 mV, due to anionic sulfate half-ester groups, indicating electrostatic stability similar to a previous study [27]. The zeta potentials of MAA5 and MAA10 latexes were measured to be −44 mV and −47 mV, respectively, attributed to the anionic surfactant (SLS) and MAA on the particle surface.

3.2. Acrylic latex/CNC composite film formation

Figure S3 shows films prepared from MAA10 latex, indicating that the CNCs did not impede film formation. The CNC-loaded films were visually similar to the neat films. The values of T_g for MAA5 and MAA10 latexes were measured with DSC to be −7 °C (MAA5) and −11 °C (MAA10). Figure S5 displays the portion of DSC heating curves highlighting the heat flow change due to the T_g. The addition of CNCs did not affect the T_g of the films in these experiments. Additionally, all composites resulted in MFFT of approximately 0 ± 0.4 °C.

The dispersion of CNCs in latex films was evaluated with PLM images, shown in Fig. 1 for neat and CNC-loaded MAA5 films. No birefringence was observed in the neat MAA5 film. The interaction of polarized light with CNCs resulted in birefringent domains of a size range suggesting CNC aggregation. Birefringence in the CNC loaded films was homogeneous and had low intensity, indicating that CNC aggregates are well-distributed in the water phase of the latex. The birefringent domains spread out and brighten with increasing CNC loadings, as expected. Similar results were observed for MAA10/CNC latex composite films (Figure S6).

PLM also gives information about whether a film is isotropic or anisotropic. Maltese cross patterns (Figure S7) were observed in both MAA5 and MAA10 composite films containing CNC loadings of 3−15 wt %. The maltese cross pattern indicates CNCs located between coalesced acrylic particles forming a spherical symmetry [28] following drying.

AFM amplitude images are given in Figure S8. All film surfaces were relatively smooth with rms roughness less than 10 nm (Table 1). The addition of CNC in each latex type increased the coating roughness by a statistically significant amount based on one-way ANOVA and t-tests (α = 0.05). MAA10/CNC films have slightly higher surface roughness than MAA5/CNC films.

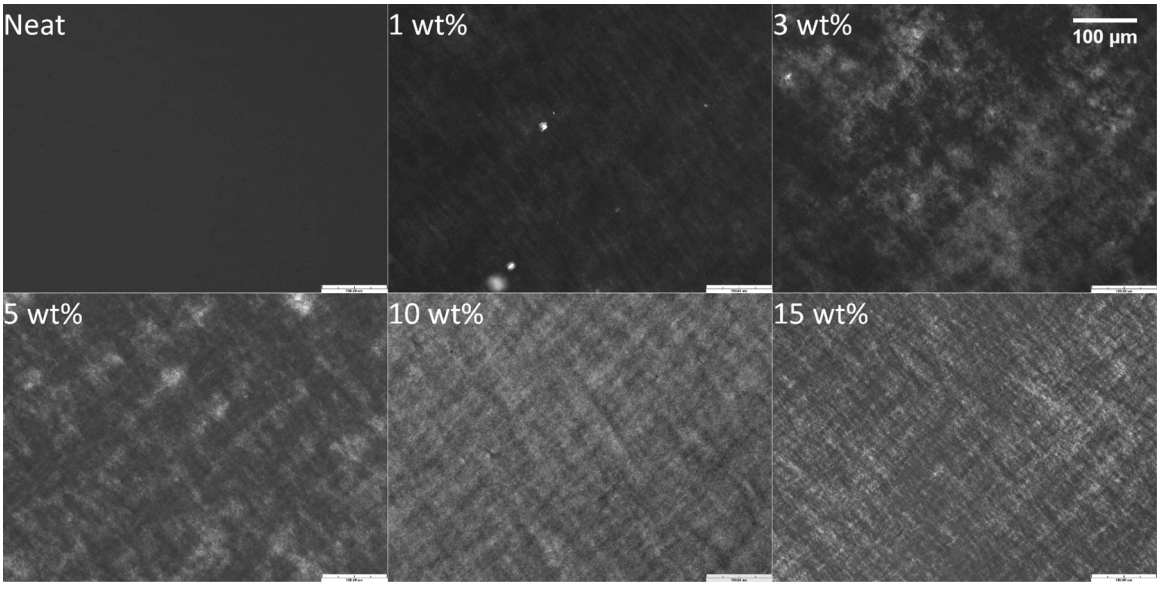

Fig. 1. Polarized light microscope images of MAA5 and MAA5/CNC composites. The scale bar is 100 μm in all images.

Table 1
Average roughness (nm) of latex/CNC composite films.

CNC loading (wt%)	Roughness (nm)	
	MAA5	MAA10
0	1.8 ± 0.6	1.9 ± 0.3
5	2.8 ± 0.3	3.5 ± 0.5
15	3.4 ± 0.3	4.5 ± 0.5

The film top surfaces did not show features related to CNC size and shape, suggesting that CNCs were located in the coating bulk. Similar behavior was reported for CNC/styrene-acrylic latex copolymer composites [18]. The negatively charged acrylic particles are unlikely to have CNCs on their surfaces because of electrostatic repulsion. During latex particle coalescence, CNCs are likely to become trapped in interstices between particles, hindering their migration to the top film surface. Limousin et al. [29] investigated the film formation of CNC/cationic acrylic latex dispersions. Because CNCs electrostatically attached to cationically-modified acrylic particles, CNCs were observed on the surface of coatings in AFM imaging.

SEM was used to confirm the location of the CNCs in the coating cross-section. Similar to the AFM imaging, no features were observed on the top surface of composite films. However, CNCs were embedded in the acrylic matrix in the cryo-fractured cross-sections (Fig. 2). Small white regions are attributed to aggregates of rod-shaped CNCs since these regions do not exist in the fractured surface of neat latex films. Similar morphology was reported in composites of CNCs with various polymers [30–32]. During the drying and coalescence of acrylic particles, CNCs are confined to interstitial regions, where they concentrate as water evaporates. CNC-CNC aggregation is to be expected because CNCs are forced into close contact as water evaporates and latex coalesces. Compression of the CNC dispersion between latex particles during drying enhances the van der Waals forces and hydrogen bonding between CNCs and causes aggregation in the latex films. The hydrogen bonding between the CNCs and carboxyl groups on the surface of latex particles is also part of the aggregation process. CNCs incorporated into soft hydrophobic styrene butadiene rubber matrices showed a similar microstructure [33], with physically connected CNCs in interstitial space between latex particles.

The diameters of the white regions were measured from SEM to be 47 ± 21 nm and 43 ± 16 nm for 5 wt% CNC loaded MAA5 and MAA10 composites, respectively. CNC-loaded MAA5 films with 15 wt% CNC had aggregates having a diameter of 37 ± 14 nm whereas 15 wt% CNC-loaded MAA10 films had aggregates with 48 ± 17 nm diameter. The aggregate size did not change significantly with the addition of CNCs; however, the density of the aggregates increased with increasing CNC content. The distance between 100 randomly selected CNC aggregates was measured from SEM images. Aggregates in MAA5 composite films were 403 ± 72 nm and 236 ± 122 far away from each other for 5 wt% and 15 wt% CNC loadings, respectively. In MAA10 the distance between aggregates was 425 ± 166 nm with 5 wt% CNC and it dropped to 233 ± 82 nm with 15 wt% CNC. Not every gap between acrylic particles had CNC confinement, which has been observed in aggregates observed in other CNC-loaded BA/MMA latex films [20].

3.3. Film transparency

The UV–vis transmittance spectra of latex/CNC films over the visible wavelength range of 400−800 nm are included in supporting information (Figure S9). The transmittance at 550 nm is shown in Table 2 and was reduced from 92.1 % to 74.3 % as CNC loading increased from 0 wt % to 15 wt% for MAA5. Behavior was similar for MAA10/CNC. The optical transmittance depends on the dispersion of CNCs in the dry latex matrix, and these changes are within ranges reported previously. For example, a transmittance of 70 % was observed in a butyl methacrylate latex film loaded with 4 wt% CNC, compared to a neat latex transmittance above 95 % [34].

Table 2
Light transmittance (%) of neat and CNC loaded latex films: a) MAA5, b) MAA10 at 550 nm.

CNC loading (wt%)	Transmittance (%)[a]	
	MAA5	MAA10
0	92.1	95.3
1	91.8	93.1
3	90.2	91.2
5	88.5	89.2
8	82.4	84.4
10	79.6	83.3
15	74.3	72.3

[a] Standard deviation was less than 2% for each measurement.

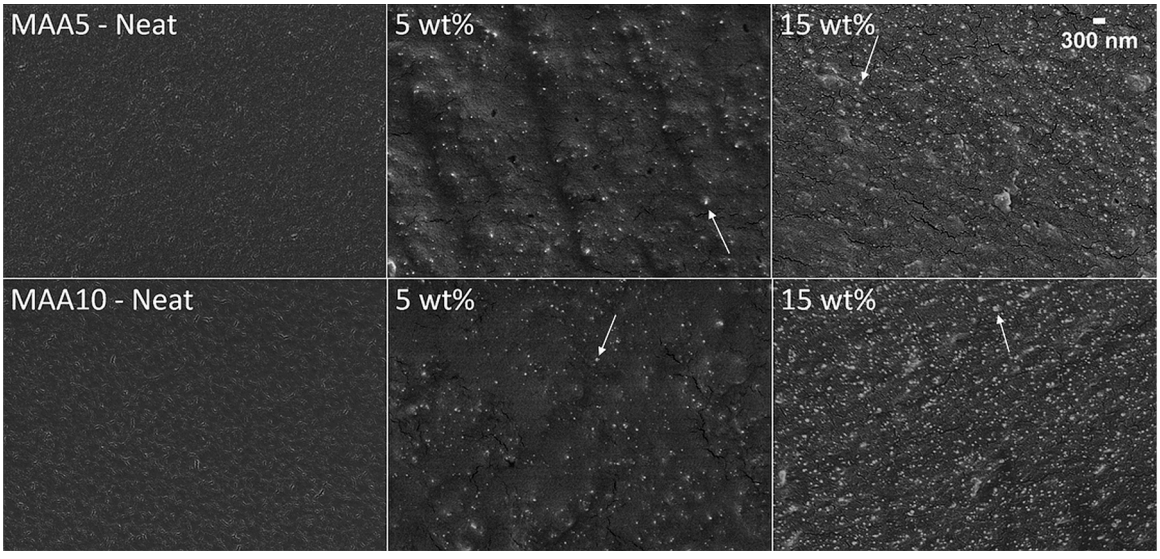

Fig. 2. SEM images of the cryo-fractured surfaces of MAA5 (top) and MAA10 (bottom) latex films. Scale bar is 300 nm and applies all images. Arrows pointing to white regions representing CNC aggregates.

3.4. Water content

Water content and CNC composition in the composite films dried at ambient temperature were determined with TGA, and the results are shown in Figure S10. Neat films had a single-step weight loss whereas CNC-loaded (5 and 15 wt%) samples showed a two-step profile. The initial weight loss increased with increasing CNC content. The onset temperature of thermal degradation for CNCs was determined to be around 290 °C from the first weight loss step. Neat latexes began degrading at around 380 °C. However, no significant weight loss was observed at around 100 °C, suggesting that an undetectable quantity of water was retained. This was further tested by drying the 5 wt% CNC loaded MAA5 and MAA10 latex films at 100 °C for three hours followed by TGA. The results were similar to those obtained after drying at ambient conditions (Figure S11), suggesting that the addition of CNCs did not change the water retention behavior.

To confirm the effect of CNCs on the water content remaining in the films after drying, FTIR spectra were collected from neat and CNC-loaded films. The spectra are shown in Figure S12. A higher absorbance at 3000−3600 cm^{-1} corresponding to −OH stretching was observed for the CNC loaded samples. The absorption for −OH could be caused by not only CNCs but also by water remaining in the films. Similar to the TGA experiments, 5 wt% CNC loaded samples were dried at 100 °C for three hours. The FTIR spectra of films dried at high and ambient temperature were compared by performing paired t-tests ($\alpha = 0.05$). We found no significant difference between the two spectra (Figure S13) suggesting that the increased intensity of the −OH was due to CNC addition and not increased water content.

3.5. Mechanical performance

Mechanical property changes due to CNC addition and latex composition were assessed using several methods. We obtained UTS and strain at break from a biaxial tensile test. The uniaxial tensile test provided stress-strain curves, from which we calculated Young's modulus values in addition to UTS and strain at break. Nanoindentation experiments produced force vs. displacement profiles of the composite films from which hardness was obtained. We performed pencil hardness and Koenig pendulum tests as well.

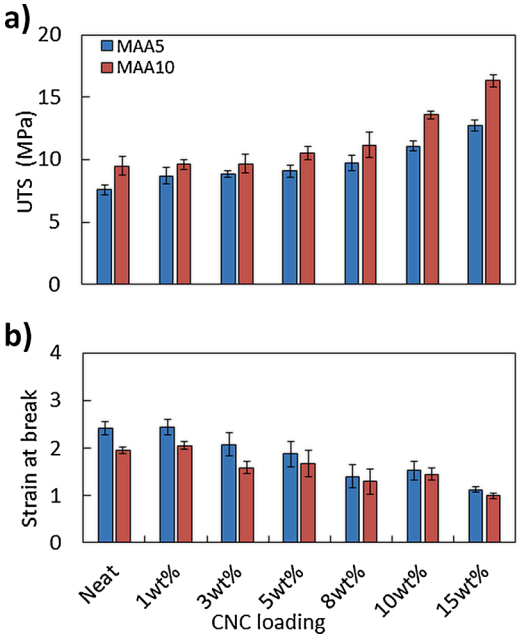

Fig. 3. Biaxial tensile test results of neat and CNC loaded latex films: a) UTS, b) strain at break.

Fig. 3 shows biaxial tensile testing results of films containing 0−15 wt% CNC. UTS increased with increasing CNC loading, whereas strain at break decreased. UTS was increased from 9 MPa to 16 MPa by loading 15 wt.% CNC compared to the neat film. MAA10 composites resulted in higher UTS and lower strain at break values compared to MAA5 composites. We confirmed that dilution of latexes with water in the CNC dispersion did not affect the results of tensile testing (Figure S14).

Fig. 4 shows strain-stress curves obtained from uniaxial tensile testing and Table S5 summarizes the calculated modulus values, which increased with the addition of CNCs. Similar to biaxial tensile results, increased CNC loading resulted in decreased strain at break and increased the UTS of the films. MAA5/CNC had slightly higher strain at failure values compared to MAA10/CNC films. The 15 wt% CNC loading increased the modulus by a factor of 30x and 40x in MAA5 and MAA10, respectively, relative to neat films. We obtained a Young's modulus ~500 MPa in 15 wt% CNC films, in the range moduli of high T_g binder used commercially [35]. Limousin et al. [20] studied composite latex/CNC films having a morphology similar to this work. Starting with a harder latex prepared with 50 wt% BA and 50 wt% MMA, the modulus increased from 37 ± 5 MPa in the neat film to 270 ± 20 MPa when the latex film was loaded with 20 wt% CNC. Further improvement could be expected if CNCs were *in situ* added during latex synthesis. Dastjerdi et al. [36] observed difference in mechanical performance of the CNC loaded pressure sensitive adhesive (PSA) films when *in situ* vs blending technique was used for the addition of CNCs. *In situ* method resulted in greater improvement in the shear resistance, tack and peek strength of the PSA films compared to results obtained from blending method. The difference in the improvements of properties was associated with the better interaction of CNCs with the latex because CNCs were mixed with the latex for a longer time at elevated temperature when *in situ* loaded.

A higher MAA composition in the latex was associated with slightly enhanced tensile strength and modulus. MAA is a water-soluble

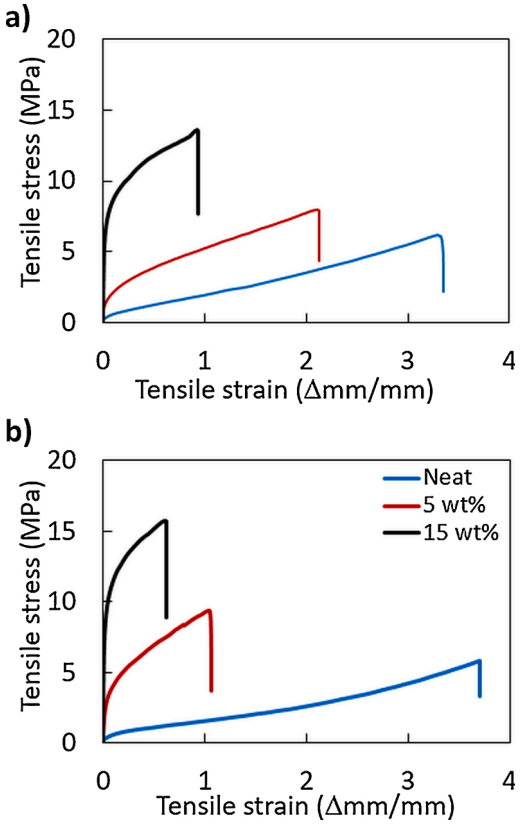

Fig. 4. Strain-Stress curves from the uniaxial tensile test of neat and CNC loaded latex films: a) MAA5 and b) MAA10.

monomer carrying a carboxyl group. The distribution of MAA in latexes is sensitive to pH of the aqueous phase, the reactivity ratios for copolymerization, and the polymerization method (batch or semi-continuous) [37]. Depending on pH at polymerization, MAA may be in the particle interior, on the particle surface or in the aqueous phase [38]. Our latexes were synthesized with the aqueous phase at pH = 3.5−4. By keeping pH just below the pKa of MAA (4.65), we aimed to distribute carboxyl groups close to the surface of particles, increasing the chance of interaction of MAAs with CNCs. After the polymerization, latexes were neutralized, and carboxyl groups were charged. MAA has various effects on film formation: (a) Charged carboxyl groups assist to the colloidal stability in latexes. The electrostatic stabilization in the latex may promote dispersion of CNCs in the latex. (b) Carboxyl groups provide hydrogen bonding and ionic dipole interactions between latex particles. Wang et al. [39] studied the pH influence of the wet carboxylated BA latex on molecular interactions in the dry films and, in turn, on their mechanical properties. At a pH of 9, they found that ionic dipolar interactions contribute to the film stiffness and cohesion more than hydrogen bonding. A study by Feng and Winnik [40] proposed that a pH drop in latexes neutralized by ammonium hydroxide during film formation was due to the evaporation of ammonia. The decrease in pH leads to protonation of carboxylate groups on the surface of particles, diminishing the ionic dipolar interactions. Therefore, we expect both mechanisms of hydrogen bonding and ionic dipolar interactions in our latexes. We also expect ammonium evaporation and a pH drop during drying of latexes, decreasing the contribution of ionic dipolar interaction to film strength. (c) Carboxyl groups on the surface of latex particles interact with hydroxyl groups on CNCs. Lu and Hsieh [25] established the existence of hydrogen bonding between acid groups and hydroxyl groups on CNC in poly(acrylic acid)/CNC nanocomposites. (d) Carboxyl groups hold water by forming hydrogen bonding with the trapped water in the film, reducing the effective T_g of polymers called hydroplasticization [41]. We think the hydroplasticization effect of MAA is limited in our case because BA composition in the latex synthesis is more than 50 %, resulting in T_g below ambient film formation temperature.

The loading and unloading force vs. displacement curves from nanoindentation experiments are reported in Fig. 5. Displacements increased with increasing peak loads in each tested latex film. Since we kept the indentation time constant, peak loads increased with increasing CNC content; however, indentation displacements became smaller even though higher loads were achieved. This result suggests improvement in film hardness with added CNC. Although the negative force values indicated adhesive interaction between the tip and the sample, the film hardness was calculated from the loading curves, which are not affected by the tip-sample adhesion.

Fig. 6 shows the hardness values of the films obtained from three different techniques. In Fig. 6a, nanoindentation curves showed a significant enhancement in hardness with CNC loading. MAA content did not significantly affect the indentation hardness. The 15 wt% CNC loadings had a hardness 10x over that of neat latex. Abitbol et al. [18] was able to increase the indentation hardness of VOC-containing styrene-acrylic latex coatings 2.5x by loading 9 wt% CNC while the hardness of neat coating was 7 MPa. We obtained the same improvement at a loading of 5 wt% CNC by increasing the hardness from 1.5 MPa to about 3−4 MPa, without use of high Tg acrylic that requires added coalescent.

The pencil hardness of the neat and CNC loaded (5 and 15 wt%) films is shown in Fig. 6b. Pencil hardness is less quantitative than nanoindentation hardness but is a common industry standard. The highest pencil grade that will neither cut nor scratch the film surface is the scratch hardness. The highest grade that will not cut through the film defines the gauge pencil hardness. All films were scratched by all grades (from softest 6B to hardest 6 H). Neat MAA5 and MAA10 latex films, and their 5 wt% CNC loaded films resulted in gauge pencil hardness of F. The 15 wt% CNC loaded films had a gauge pencil hardness of H, an improvement of one pencil grade.

CNC loaded latexes were also tested for the Koenig hardness, which is an industry-standard test for coatings. A typical coalescent-containing hard acrylic film toughens over days, and hardness increases from the 1st to 7th day after the coating application. During this period, coalescent evaporates into the air. A benchmark hard acrylic containing coalescent gives a Koenig hardness of 31 s in the 1st day and 47 s in the 7th day [42]. The Koenig hardness results are given in Fig. 6c for CNC loaded coalescent-free MAA5 acrylic formulation. CNC loading improved the hardness in the 1st day at all compositions. The addition of 15 wt% CNC into neat MAA5 latex increased the hardness to 37.3 s (Fig. 6c). No difference was observed between readings of 1st and 7th day in the CNC loaded latexes because no evaporative coalescent was present.

Santos et al. [43] studied the effect of three types of coalescent on MFFT, coalescence and Koenig hardness of acrylic paint formulations. Pure acrylic latex having a MFFT of 17 °C was used. The coalescents were divided into three categories based on VOC content: 100 g/L, 50

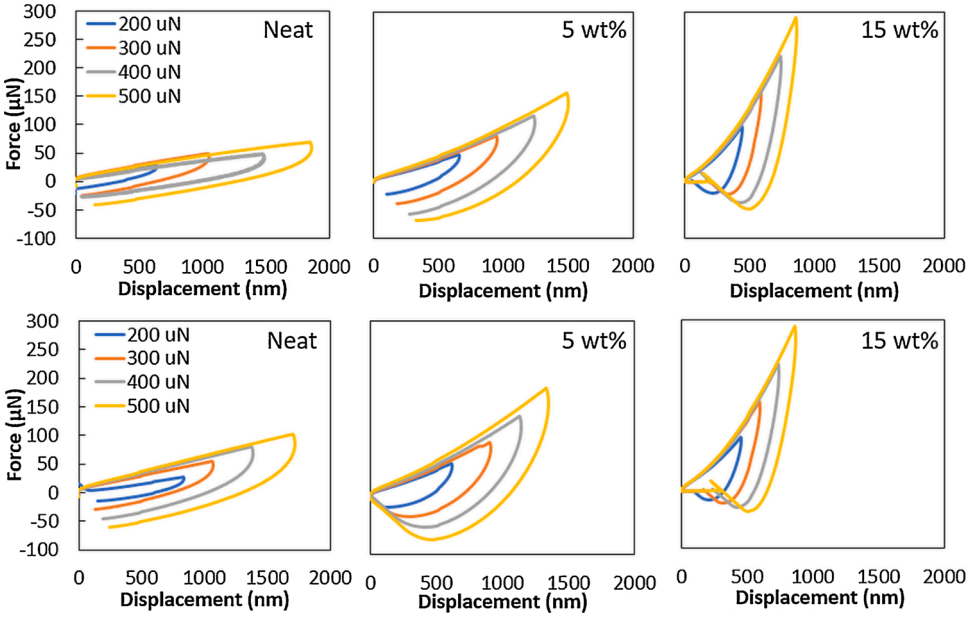

Fig. 5. Force vs. displacement plots from nanoindentation: MAA5 (top) and MAA10 (bottom) at different loading forces.

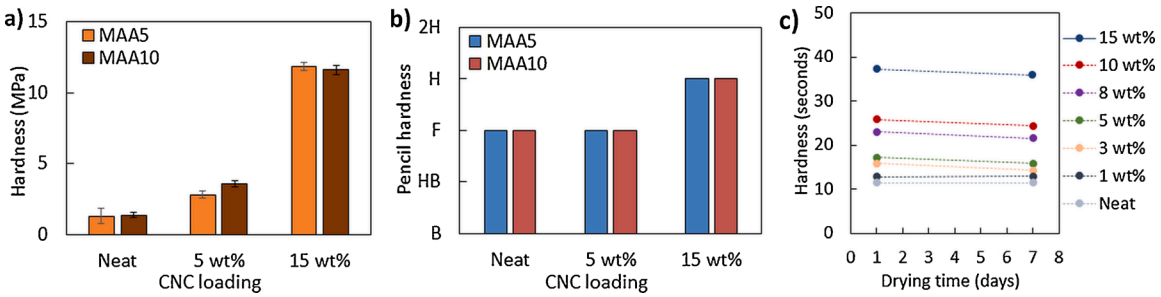

Fig. 6. Hardness values obtained from a) nanoindentation, b) pencil hardness test, c) Koenig pendulum test.

g/L, and zero VOC. Coalescents containing 100 g/L VOC were organic solvents that favor the interdiffusion of polymer particles. The 50 g/L and zero VOC coalescents contain solvents with high molecular weights and boiling points. They remain in the latex films after drying and negatively affect the hardness of the coatings. All coalescents resulted in decreased MFFT in a similar manner. Better coalescence was observed in AFM images for latex films containing 50 g/L and zero VOC coalescent. However, zero-VOC coalescent resulted in poor hardness evolution, decreasing the Koenig hardness approximately 50 % compared to the latex with 100 g/L VOC. While the zero VOC high molecular weight coalescent plasticizer negatively affected hardness evolution in that work, the approach using soft acrylic with up to 15 wt% CNC loading enhanced the Koenig hardness almost 230 % relative to neat films without compromising film coalescence.

The use of CNCs in this work enhanced the mechanical performance of soft latex films to an extent similar to other colloidally-stable, hard nanofillers. However, using CNCs may be more attractive for sustainability because CNCs are renewably-sourced. As a way to assess the benefits of this approach, the results obtained here are compared to literature results with a common hard mineral nanoparticle, silica. Silica nanoparticles have some similarities to CNCs, facilitating this comparison. Both CNCs and silica particles are stiff materials with high surface area and hydroxyl-rich surfaces. Additionally, silica has been frequently used as a reinforcing agent in waterborne latexes. Ramos-Fernández et al. [44] *in situ* incorporated colloidal silica (7 nm particle size) into the aqueous phase of BA/MMA latexes. Silica nanoparticles were adsorbed on the surface of the latex particles. The 20 wt% silica loading increased nanoindentation modulus to 1.25 GPa from 0.4 GPa (neat film) (~3X improvement). Abitbol et al. blended fumed silica (10 nm primary particles) and CNC (110 ± 7 nm x 7.5 ± 0.5 nm) into a waterborne styrene-acrylic latex separately. The measured hardness of 2–5 wt% CNC loaded films was similar to the hardness of 9 wt% silica loaded film, suggesting more efficient reinforcement with CNCs.

CNCs have low to negligible toxicity based on a recent review [45]. Despite the limited number of studies, CNCs have thus far been found to be non-toxic upon ingestion or contact with skin. The health effects on inhalation and cytotoxicity are less conclusive because of the different physicochemical properties of CNCs from different sources and impurities remaining after their production.

A few life cycle assessment (LCA) studies [46–48] were performed to understand the environmental impacts of nanocellulose production and to guide its industrialization efforts. Energy optimization in CNC production has progressed slowly due to immaturity of the production technology. One challenge in interpreting LCA studies available is that the initial refinement from biomass to pulp containing at least 85 wt% cellulose [49] is done at paper mills, but available LCA studies considers pulp as the starting material. Additionally, ~65 % of energy consumption [46] in CNC production after pulping is from producing sulfuric acid used for hydrolysis of cellulose and sodium hydroxide used to neutralize the acid after the hydrolysis. Researchers have been working on techniques [50] to increase the production yield and reducing acid or base used, including recovery of hydrolyzing acid [51], integration of nanocellulose production with pulping processes [52], the AVAP® technology from American Process Inc. [53] and R3™ technology from Blue Goose Biorefineries [54].

4. Conclusions

We reinforced coalescent-free BA/MMA/MAA latexes with CNCs by a simple blending method. Due to the high composition of BA in the formulations, the latexes formed uniform films at ambient conditions. All coatings had a MFFT of 0 °C, and T_g lower than MFFT, regardless of CNC loading. SEM imaging suggested that the CNCs were confined to interstitial regions between latex particles, and these collections of CNCs were distributed through the bulk of the film. Film transparencies in the range of 93.1–72.3 % were obtained in films loaded with 1–15 wt% CNC. CNC loadings significantly enhanced the tensile strength, Young's modulus, and hardness without negatively affecting ambient film formation. We obtained slightly higher tensile strength and Young's modulus measurements in the latex films with higher MAA content. A 10x improvement was achieved in the nanoindentation hardness with the addition of 15 wt% CNCs. The composite films reached maximum hardness in the first day of drying without coalescent. This work highlights the remarkable effect of CNC addition on the mechanical performance of coalescent-free latex coatings. The mechanical properties achieved are comparable with the conventional binders that use VOC coalescents with hard acrylic polymers and exceed properties (such as Koenig hardness) of binders that use non-volatile coalescents that remain in the coating. The CNC loaded nanocomposite latexes studied in this work are potential binders useful for the development of zero-VOC waterborne acrylic coatings. The use of CNCs does lead to questions about the interaction of the CNC with other components (beyond the binder) used in commercial formulations. While the scope of this study is focused on the binder itself, it encourages reformulating studies of waterborne acrylic products with CNCs.

CRediT authorship contribution statement

Ezgi M. Dogan-Guner: Methodology, Validation, Formal analysis, Investigation, Visualization, Writing - original draft, Writing - review & editing. **Stan Brownell:** Conceptualization, Investigation, Resources, Supervision, Writing - review & editing. **Gregory T. Schueneman:** Conceptualization, Resources, Supervision, Writing - review & editing. **Meisha L. Shofner:** Conceptualization, Supervision, Writing - review & editing. **J. Carson Meredith:** Conceptualization, Supervision, Writing - review & editing.

Declaration of Competing Interest

The authors reported no declarations of interest.

Acknowledgements

This research was financially supported by P^{3}Nano program in the

US Endowment for Forestry and Communities (Grant 16-JV-11111106-052). The authors of this paper would like to thank the USDA Forest Service Forest Products Laboratory (FPL) and Dow Chemical for their collaboration. This work was performed in part at the Georgia Tech Institute for Electronics and Nanotechnology, a member of the National Nanotechnology Coordinated Infrastructure, which is supported by the National Science Foundation (Grant ECCS-1542174).

Appendix A. Supplementary data

Supplementary material related to this article can be found, in the online version, at doi:https://doi.org/10.1016/j.porgcoat.2020.105969.

References

[1] Paints and Coatings Market by Product (High Solids, Powder, Waterborne, Solvent-borne), by Material (Acrylic, Alkyd, Polyurethane, Epoxy & Polyesters), by Application, and Segment Forecasts, 2018 - 2025, Grand View Research, 2017.
[2] US EPA Archive Document - Paint and Coatings, 2019. April 17, 2019]; Available from: https://archive.epa.gov/sectors/web/pdf/paintandcoatings-2.pdf.
[3] A. Pennock, et al., Selecting Green Paint, 2014 March 12, 2019]; Available from:, 2019 https://greenhomeguide.com/know-how/article/selecting-green-paint.
[4] United States Environmental Protection Agency, Volatile Organic Compounds' Impact on Indoor Air Quality, March 12, 2019]; Available from:, 2019 https://www.epa.gov/indoor-air-quality-iaq/volatile-organic-compounds-impact-indoor-air-quality.
[5] The Society for Protetice Coatings Learning Center - VOC Regulations and Why They Matter for Your Next Coating Project, 2019. April 17, 2019]; Available from: https://www.sspc.org/learning_center/voc-regulations-and-why-they-matter-for-your-next-coating-project/.
[6] United States Environmental Protection Agency, Ground-level Ozone Pollution, March 12, 2019]; Available from:, 2019 https://www.epa.gov/ground-level-ozone-pollution/ground-level-ozone-basics.
[7] Y. Wang, M.A. Winnik, Effect of a coalescing aid on polymer diffusion in latex films, Macromolecules 23 (21) (1990) 4731–4732, https://doi.org/10.1021/ma00223a038.
[8] F. Hussain, et al., Review article: polymer-matrix nanocomposites, processing, manufacturing, and application: an overview, J. Compos. Mater. 40 (17) (2006) 1511–1575, https://doi.org/10.1177/0021998306067321.
[9] R. Babu Valapa, et al., Chapter 2 - an overview of polymer–clay nanocomposites, in: K. Jlassi, M.M. Chehimi, S. Thomas (Eds.), Clay-Polymer Nanocomposites, Elsevier, 2017, pp. 29–81.
[10] S. Meer, A. Kausar, T. Iqbal, Attributes of polymer and silica nanoparticle composites: a review, Polym. Technol. Eng. 55 (8) (2016) 826–861, https://doi.org/10.1080/03602559.2015.1103267.
[11] Z. Spitalsky, et al., Carbon nanotube–polymer composites: chemistry, processing, mechanical and electrical properties, Prog. Polym. Sci. 35 (3) (2010) 357–401, https://doi.org/10.1016/j.progpolymsci.2009.09.003.
[12] R.J. Moon, et al., Cellulose nanomaterials review: structure, properties and nanocomposites, Chem. Soc. Rev. 40 (7) (2011) 3941–3994, https://doi.org/10.1039/C0CS00108B.
[13] K.-Y. Lee, Nanocellulose and Sustainability: Production, Properties, Applications, and Case Studies. Nanocellulose and Sustainability: Production, Properties, Applications, and Case Studies, CRC Press, 2018, pp. 1–295.
[14] R.J. Moon, G.T. Schueneman, J. Simonsen, Overview of cellulose nanomaterials, their capabilities and applications, JOM 68 (9) (2016) 2383–2394, https://doi.org/10.1007/s11837-016-2018-7.
[15] S.J. Eichhorn, et al., Review: current international research into cellulose nanofibres and nanocomposites, J. Mater. Sci. 45 (1) (2010) 1–33, https://doi.org/10.1007/s10853-009-3874-0.
[16] C. Miao, W. Hamad, Cellulose reinforced polymer composites and nanocomposites: a critical review, Cellulose 20 (2013), https://doi.org/10.1007/s10570-013-0007-3.
[17] S. Xu, et al., Mechanical and thermal properties of waterborne epoxy composites containing cellulose nanocrystals, Polymer 54 (24) (2013) 6589–6598, https://doi.org/10.1016/j.polymer.2013.10.011.
[18] T. Abitbol, et al., Comparison of nanocrystalline cellulose and fumed silica in latex coatings, Green Mater. 2 (4) (2014) 206–221, https://doi.org/10.1680/gmat.14.00017.
[19] Y. Pu, et al., Investigation into nanocellulosics versus acacia reinforced acrylic films, Compos. Part B Eng. 38 (3) (2007) 360–366, https://doi.org/10.1016/j.compositesb.2006.07.008.
[20] E. Limousin, et al., Linking film structure and mechanical properties in nanocomposite films formed from dispersions of cellulose nanocrystals and acrylic latexes, Langmuir 36 (8) (2020) 2052–2062, https://doi.org/10.1021/acs.langmuir.9b03861.
[21] S. Beck-Candanedo, M. Roman, D.G. Gray, Effect of reaction conditions on the properties and behavior of wood cellulose nanocrystal suspensions, Biomacromolecules 6 (2) (2005) 1048–1054, https://doi.org/10.1021/bm049300p.
[22] A.Y.C. Koh, et al., The influence of copolymerization with methacrylic acid on poly (butyl acrylate) film properties, Polymer 47 (4) (2006) 1159–1165, https://doi.org/10.1016/j.polymer.2005.12.053.
[23] C. Akarsu Dülgar, İ.E. Serhatlı, Synthesis of poly(BA-co-MMA) dispersions having AA/MAA/AAm/MAAm comonomers and the comparison of their effect on adhesive performance, Polym. Bull. 75 (2) (2018) 877–890, https://doi.org/10.1007/s00289-017-2055-6.
[24] J. Yang, et al., Revealing strong nanocomposite hydrogels reinforced by cellulose nanocrystals: insight into morphologies and interactions, ACS Appl. Mater. Interfaces 5 (24) (2013) 12960–12967, https://doi.org/10.1021/am403669n.
[25] P. Lu, Y.-L. Hsieh, Cellulose nanocrystal-filled poly(acrylic acid) nanocomposite fibrous membranes, Nanotechnology 20 (41) (2009) 415604, https://doi.org/10.1088/0957-4484/20/41/415604.
[26] J.-L. Sormana, S. Chattopadhyay, J.C. Meredith, High-throughput mechanical characterization of free-standing polymer films, Rev. Sci. Instrum. 76 (6) (2005) 062214, https://doi.org/10.1063/1.1926967.
[27] M.S. Reid, M. Villalobos, E.D. Cranston, Benchmarking cellulose nanocrystals: from the laboratory to industrial production, Langmuir 33 (7) (2017) 1583–1598, https://doi.org/10.1021/acs.langmuir.6b03765.
[28] S. Kalia, B.S. Kaith, I. Kaur, Cellulose Fibers: Bio- and Nano- Polymer Composites. Green Chemistry and Technology, Springer, 2011.
[29] E. Limousin, N. Ballard, J.M. Asua, Synthesis of cellulose nanocrystal armored latex particles for mechanically strong nanocomposite films, Polym. Chem. 10 (14) (2019) 1823–1831, https://doi.org/10.1039/C8PY01785A.
[30] G. Siqueira, et al., Cellulose nanocrystal inks for 3D printing of textured cellular architectures, Adv. Funct. Mater. 27 (12) (2017) 1604619, https://doi.org/10.1002/adfm.201604619.
[31] P.-X. Wang, W.Y. Hamad, M.J. MacLachlan, Structure and transformation of tactoids in cellulose nanocrystal suspensions, Nat. Commun. 7 (2016) 11515, https://doi.org/10.1038/ncomms11515.
[32] L. Tang, C. Weder, Cellulose Whisker/Epoxy resin nanocomposites, ACS Appl. Mater. Interfaces 2 (4) (2010) 1073–1080, https://doi.org/10.1021/am900830h.
[33] P.K. Annamalai, et al., Water-responsive mechanically adaptive nanocomposites based on Styrene–butadiene rubber and cellulose nanocrystals—processing matters, ACS Appl. Mater. Interfaces 6 (2) (2014) 967–976, https://doi.org/10.1021/am404382x.
[34] A. Ben Mabrouk, et al., Synthesis and characterization of cellulose whiskers/polymer nanocomposite dispersion by mini-emulsion polymerization, J. Colloid Interface Sci. 363 (1) (2011) 129–136, https://doi.org/10.1016/j.jcis.2011.07.050.
[35] L. Podgorski, M. de Meijer, J.D. Lanvin, Influence of coating formulation on its mechanical properties and cracking resistance, Coatings 7 (10) (2017), https://doi.org/10.3390/coatings7100163.
[36] Z. Dastjerdi, E.D. Cranston, M.A. Dubé, Pressure sensitive adhesive property modification using cellulose nanocrystals, Int. J. Adhes. Adhes. 81 (2018) 36–42, https://doi.org/10.1016/j.ijadhadh.2017.11.009.
[37] T. Ding, et al., Synthesis and characterization of functionalized polymer latex particles through a designed semicontinuous emulsion polymerization process, J. Appl. Polym. Sci. 97 (1) (2005) 248–256, https://doi.org/10.1002/app.21678.
[38] A.M. Santos, J. Guillot, T.F. McKenna, Partitioning of styrene, butyl acrylate and methacrylic acid in emulsion systems, Chem. Eng. Sci. 53 (12) (1998) 2143–2151, https://doi.org/10.1016/S0009-2509(98)00031-1.
[39] T. Wang, et al., pH dependence of the properties of waterborne pressure-sensitive adhesives containing acrylic acid, ACS Appl. Mater. Interf. 1 (3) (2009) 631–639, https://doi.org/10.1021/am800179y.
[40] rJ. Feng, M.A. Winnik, Effect of water on polymer diffusion in latex films, Macromolecules 30 (15) (1997) 4324–4331, https://doi.org/10.1021/ma970174+.
[41] B. Voogt, et al., Film formation of high tg latex using hydroplasticization: explanations from NMR relaxometry, Langmuir 35 (38) (2019) 12418–12427, https://doi.org/10.1021/acs.langmuir.9b01353.
[42] Dow Coating Materials, Lower VOC-Faster Dry Time-Higher Productivity, July 17, 2019]; Available from:, 2019 http://msdssearch.dow.com/PublishedLiteratureDOWCOM/dh_08c0/0901b803808c0792.pdf?filepath=dcc_na/pdfs/noreg/884-00023.pdf&fromPage=GetDoc.
[43] P. Santos, et al., Low-VOC Coalescents. Coating World - Technical Paper, p, 2019, https://www.coatingsworld.com/issues/2019-2008-2001/view_technical-papers/low-voc-coalescents/.
[44] J.M. Ramos-Fernández, et al., Synthesis of poly-(BA-co-MMA) latexes filled with SiO2 for coating in construction applications, Prog. Org. Coat. 72 (3) (2011) 438–442, https://doi.org/10.1016/j.porgcoat.2011.05.017.
[45] R. Maren, Toxicity of cellulose nanocrystals: a review, Ind. Biotechnol. 11 (1) (2015) 25–33, https://doi.org/10.1089/ind.2014.0024.
[46] H. Gu, et al., LCA study for pilot scale production of cellulose nano crystals (CNC) from wood pulp, LCA XV Paper Proceedings – A Bright Green Future (2013).
[47] R. Arvidsson, D. Nguyen, M. Svanström, Life cycle assessment of cellulose nanofibrils production by mechanical treatment and two different pretreatment processes, Environ. Sci. Technol. 49 (11) (2015) 6881–6890, https://doi.org/10.1021/acs.est.5b00888.
[48] Q. Li, et al., Nanocellulose life cycle assessment, ACS Sustain. Chem. Eng. 1 (8) (2013) 919–928, https://doi.org/10.1021/sc4000225.
[49] C.A. de Assis, et al., Conversion economics of forest biomaterials: risk and financial analysis of CNC manufacturing, Biofuels Bioprod. Biorefining 11 (4) (2017) 682–700, https://doi.org/10.1002/bbb.1782.
[50] H. Xie, et al., Recent strategies in preparation of cellulose nanocrystals and cellulose nanofibrils derived from raw cellulose materials, Int. J. Polym. Sci. 2018 (2018) 7923068, https://doi.org/10.1155/2018/7923068.

[51] L. Chen, et al., Highly thermal-stable and functional cellulose nanocrystals and nanofibrils produced using fully recyclable organic acids, Green Chem. 18 (13) (2016) 3835–3843, https://doi.org/10.1039/C6GC00687F.
[52] Q.Q. Wang, et al., Approaching zero cellulose loss in cellulose nanocrystal (CNC) production: recovery and characterization of cellulosic solid residues (CSR) and CNC, Cellulose 19 (6) (2012) 2033–2047, https://doi.org/10.1007/s10570-012-9765-6.
[53] K. Nelson, et al., in: L.D. Madsen, E.B. Svedberg (Eds.), American Process: Production of Low Cost Nanocellulose for Renewable, Advanced Materials Applications, in Materials Research for Manufacturing: An Industrial Perspective of Turning Materials into New Products, Springer International Publishing, Cham, 2016, pp. 267–302.
[54] Blue Goose Biorefineries Inc, R3™technology, April 17, 2019]; Available from:, 2019 https://bluegoosebiorefineries.com/process/.